

EPJ E

Soft Matter and
Biological Physics

EPJ.org
your physics journal

Eur. Phys. J. E (2016) **39**: 131

DOI 10.1140/epje/i2016-16131-5

Toward the observation of a liquid-liquid phase transition in patchy origami tetrahedra: a numerical study

Simone Ciarella, Oleg Gang and Francesco Sciortino

edp sciences



Springer

Toward the observation of a liquid-liquid phase transition in patchy origami tetrahedra: a numerical study

Simone Ciarella^{1,a}, Oleg Gang², and Francesco Sciortino¹

¹ Dipartimento di Fisica, Sapienza Università di Roma, Piazzale Aldo Moro 2, 00185 Roma, Italy

² Chemical Engineering Department, Columbia University, 817 Mudd, New York, USA

Received 4 October 2016 and Received in final form 28 November 2016

Published online: 27 December 2016 – © EDP Sciences / Società Italiana di Fisica / Springer-Verlag 2016

Abstract. We evaluate the phase diagram of a model of tetrameric particles where the arms of the tetrahedra are made by six hard cylinders. An interacting site is present on each one of the four vertices allowing the particles to form a bonded network. These model particles provide a coarse-grained but realistic representation of recently synthesised DNA origami tetrahedra. We show that the resulting network is sufficiently empty to allow for partial interpenetration and it is sufficiently flexible to avoid crystallisation (at least on the numerical time scale), satisfying both criteria requested for the observation of a liquid-liquid critical point in tetrahedrally coordinated particles. Grand-canonical simulations provide evidence that, *in silico*, the model is indeed characterised, in addition to the gas-liquid transition, by a transition between two distinct liquid phases. Our results suggest that an experimental observation of a liquid-liquid transition in a colloidal system can be achieved in the near future.

1 Introduction

Debate on the possibility of a liquid-liquid (LL) phase transition in one-component systems is still active [1–9]. Starting from the initial observation of a van der Waals loop at supercooled temperatures (T) in numerical simulations [10] of a rigid water model (the ST2 potential [11]), several models of particles have been investigated, from primitive models [12–14] to more refined representation of tetrahedrally prone atomic systems (carbon [15,16], silicon [17–20], silica [21,22]), searching for evidence and support of the LL critical point (LLCP) thermodynamic scenario. Experimental attempts to directly reveal the LLCP in one-component systems, especially in water, have failed, mostly due to the nucleation of the samples into the stable ice phase. Indeed for water the supposed critical point, if exists, is located in a region where the liquid is strongly metastable with respect to the crystal, in the so-called “No man’s land” [23]. This region is limited by homogeneous nucleation from high T and by the glass transition from low T , preventing any practical measurement and thwart direct experiments aimed at exploring the critical point. Experimental evidence based on approaching the no-man’s land from the glass side strongly supports the existence of two distinct liquid phases [24–27].

According to simulations, the two liquid phases differ in their local density and local ordering. The low den-

sity phase can be considered as a realisation of a random tetrahedral network [28], in which all particles participate in four bonds, but in a disordered structure. The denser phase is also characterized by an extended network formed by more distorted and strained bonds. Ideally, in very soft potentials, the dense phase is associated to two inter-penetrated networks, which retain their individuality only up to the third bonded neighbour distance [29]. It has been shown that the possibility to generate two inter-penetrated disordered network structures (*e.g.* the softness of the pair interaction potential) favours the onset of a liquid-liquid transition [30–32]. Recent theoretical and numerical work has attempted to quantify the parameters in the interaction potential controlling the extension of the no-man’s land and the relative stability of the liquid as compared to the crystal phase in tetrahedral particles. It has been shown that crystal nucleation in hexagonal (and cubic) diamond structures is very sensitive to the directionality of the intra-particle bonds [33, 34]. If bonds are highly flexible the configurational entropy (*e.g.* the number of distinct bonding patterns) monopolizes the total entropy of the system promoting a liquid phase which remains stable down to vanishing temperatures [35]. Interestingly, it has been shown [31,36,37] that bond flexibility also suppresses the liquid-liquid transition, but at a slower pace, offering the possibility to generate conditions in which it is possible to observe the LLCP in the absence of crystallization. Thus *softness* (*e.g.* ability

^a e-mail: simoneciarella@gmail.com

to inter-penetrate) and bond *flexibility* appear to be the crucial ingredients for giving rise to a one-component system which displays an experimentally accessible (*e.g.* in equilibrium as opposed to metastable equilibrium) liquid-liquid critical point. This implicitly suggests that within the realm of soft matter—where a detailed control of particle shape and interactions, coupled to bulk production of the particles themselves, is possible—a system of colloidal particles with a clear experimentally detectable LLCP can in principle be realized.

As an intermediate step in the direction of realising an experimental system displaying a liquid-liquid transition we provide here a numerical evaluation of the phase behaviour of rigid tetrameric structures with sticky attractive corners, mimicking both in shape and in inter-particle interaction recently synthesised nano-metric DNA origami constructs. Specifically, Liu *et al.* [38] were able to manufacture a DNA tetrahedral cage-like structure using DNA origami technique. The six “arms” of the structure are made by sticking together ten double strand helices of DNA which act as rigid cylinders, measuring approximately 8.3 nm \times 36 nm. Single strands of DNA are attached at the four vertices of the tetrahedron, to provide *T*-controlled adhesion between vertices of distinct tetrahedra. Liu *et al.* [38] manufactured these particles to link them to gold DNA-coated nanospheres to create a diamond superlattice of nano-objects via self-assembly and to realize two variant diamond lattices.

The numerical results reported in this article confirm the possibility to observe both the standard gas-liquid critical point and the liquid-liquid one. They prove that the tetrahedron shape succeeds in generating the requested “softness” (*e.g.* that it is possible to interpenetrate two different fully bonded networks without hard-core overlaps). The present results will provide a guidance for future experimental work aiming at the laboratory observation of a liquid-liquid critical point in tetrahedral particles.

2 The model

We present here a coarse-grained model for the tetrahedron origami, sketched in fig. 1. The bundle of 10 DNA helices [38] forming each of the six sides is modelled as an hard cylinder with diameter 8.3 nm and length 36 nm, as in the experiment. Six of those cylinders with fixed relative orientations define the particle structure. To model the interaction between vertices of distinct tetrahedra, experimentally realised via self-complementary DNA binding, we introduce a square-well site-site interaction of depth ϵ and width Δ . The interacting site is located at the intersection of the three cylinder axis. The energy scale ϵ is selected as unit of energy. The square-well range Δ is fixed to 6.22 nm, consistent with a length of DNA base pairs attached to each vertex of about six nucleotides. This range satisfies the single-bond-per-site condition. We note on passing that in the experimental system, the binding DNA sequences could perhaps also be engineered to favour specific relative orientations between bonded tetrahedra.

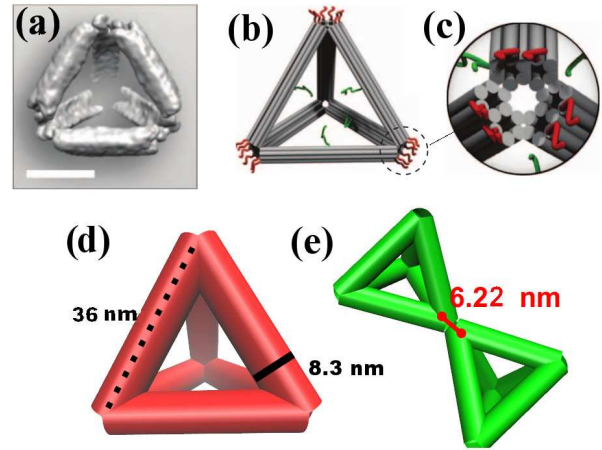


Fig. 1. (a) Cryo-electron microscopy scan of an origami tetrahedron. (b) Sketch of the self-assembled origami. (c) Detailed sketch of the origami corner. Panels (a-c) are redrawn from ref. [38]. (d) Sketch of the particle investigated in the present study. It is composed of 6 rigidly connected hard cylinders. The diameter of each cylinder measures 8.3 nm and its length is 36 nm. (e) Sketch of two bonded particles via the interaction site located on each of the four vertexes. A bond with energy ϵ is formed when the interacting sites of two distinct particles are closer than 6.22 nm.

3 Numerical methods

3.1 Standard Monte Carlo simulations in the NVT ensemble

We perform canonical Monte Carlo simulations to investigate the diamond and BCC crystals (defined by the position of the particle center of mass). We generate configurations with a total number of particles $N = 216$ (cube of length $L = 350$ nm) and $N = 250$ ($L = 270$ nm) respectively. To probe the crystal stability we run simulations at $k_B T / \epsilon = 0.063$ verifying that all possible bonds remain formed. On the fully bonded networks we measure the structure factor, the radial distribution function and the angular bond flexibility [39].

3.2 Successive umbrella sampling simulations in the μ VT ensemble

We perform grand-canonical successive umbrella sampling (SUS) simulations [40] in a cubic box of side length $L = 250$ nm with periodic boundary conditions at different T . In this method, the probability of finding N particles in the box (with $0 < N < N_{\max}$) is rebuilt joining the relative probabilities $P(N + 1)/P(N)$ evaluated in N_{\max} distinct grand-canonical simulations in which N is constrained to fluctuate between the N and $N + 1$ values. This method capitalizes on parallel computing, since each node can evaluate a distinct probability ratio. In addition, $P(N + 1)/P(N)$ can be made order one with an appropriate choice of the chemical potential μ (or equivalently activity z), significantly reducing the numerical error. For

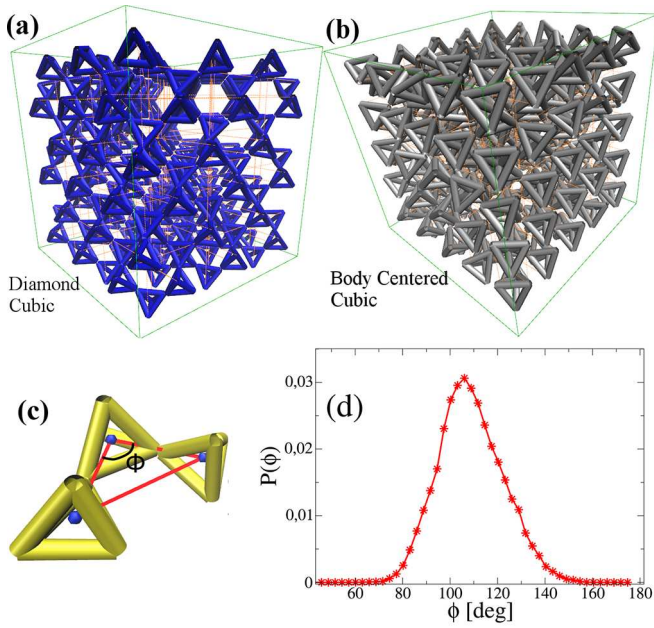


Fig. 2. Representation of (a) diamond and (b) BCC lattices formed by the studied particle. (c) Visual definition of the angle Φ , the angle between bonded triplets. The blue sphere indicates the center of mass of the particle. (d) Distribution of the angle Φ that is used to estimate flexibility [39]. The variance of the distribution provides a measure of bond flexibility. Data refer to a simulation in the liquid phase at $k_B T/\epsilon = 0.077$ and $\rho = 6.27 \cdot 10^{-6} \text{ nm}^{-3}$.

each T , $P(N)$ can be re-weighted to a different μ value to explore the desired average system density. In our calculations, we select $N_{\text{max}} = 180$, corresponding to a maximum tetrahedra number density $\rho = 1.152 \cdot 10^{-5} \text{ nm}^{-3}$.

4 Results and discussions

4.1 Softness and flexibility

To provide evidence that the shape of the particle is soft enough to allow for interpenetration of two different networks we build both diamond ($\rho_{\text{diam}} = 5.66 \cdot 10^{-6} \text{ nm}^{-3}$) and BCC ($\rho_{\text{BCC}} = 1.21 \cdot 10^{-5} \text{ nm}^{-3}$)—which is composed of two inter-penetrated diamond structures—lattices putting in a randomly oriented particle on each lattice site. A MC simulation at $k_B T/\epsilon = 0.063$ with only rotational moves shows that particle rotations quickly generated fully bonded structures in both cases. Figure 2(a), (b) show the resulting structures.

The angular bond flexibility can be estimated [39] by evaluating the bond angle distribution $P(\Phi)$. This quantity is defined as the probability to find an angle Φ between a triplet of bonded tetramers as depicted in fig. 2(c). The distribution, reported in fig. 2(d) for a liquid state at the optimal network density (*e.g.* for $\rho \approx \rho_{\text{diam}}$), is well represented by a curve centred around 108.8, close to the tetrahedral value 109.5° with variance $\sigma_\Phi = 13.6$. The width of the distribution provides a measure of the bond

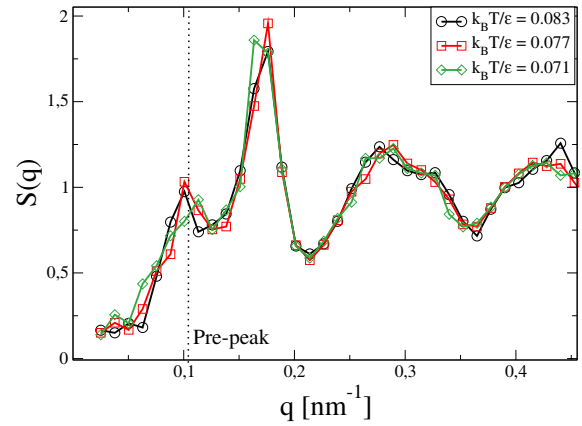


Fig. 3. Structure factor $S(q)$ from low T simulations in the liquid phase at $\rho = 6.27 \cdot 10^{-6} \text{ nm}^{-3}$. Note the pre-peak, an indication of tetrahedral order.

flexibility [39]. The observed σ_Φ value corresponds to an angular opening in an equivalent patchy particle model of $\theta_{\text{max}} = 21^\circ$ ($\cos \theta_{\text{max}} = 0.93$). For this flexibility value, LLC is expected to be weakly metastable compared to the crystal phase and hence accessible in simulations and experiments.

As a further test of the directionality of the bond between particles, fig. 3 shows the structure factor $S(q)$ between the centres of the tetrahedra evaluated in the liquid phase at $\rho = 6.27 \cdot 10^{-6} \text{ nm}^{-3}$. $S(q)$ is defined as [41]

$$S(q) \equiv \frac{\langle \rho_{\mathbf{q}} \rho_{-\mathbf{q}} \rangle}{N}, \quad (1)$$

where $\rho_{\mathbf{q}} = \sum_{i=1}^N \exp(-i\mathbf{q} \cdot \mathbf{r}_i)$, $\langle \dots \rangle$ denotes the ensemble average and the average over wave vectors \mathbf{q} with the same modules $q \equiv \|\mathbf{q}\|$, reflecting rotational invariance. \mathbf{r}_i indicates the center-of-mass position of particle i . The calculated $S(q)$ shows the pre-peak structure typical of tetrahedral liquids, originating from next-nearest-neighbour ordering imposed by the bond directionality. As for the variance of $P(\Phi)$ the amplitude of the pre-peak provides an estimate of the bond flexibility [39]. The presence of a clear pre-peak confirms the presence of a detectable tetrahedral local order.

4.2 Density dependence of the potential energy

In square-well based models, the energy provides a direct counting of the number of bonds per particle in the system. Its density dependence, at constant T , is particularly informative. Previously investigated models of tetrahedral particles [33, 42–44] show that at low T the potential energy displays a non-monotonic dependence on ρ , with a well-defined minimum at the so-called optimal network density, signalling the density at which the geometrical constraints allow for the formation of an unstrained fully bonded disordered network. The position of the minimum is usually close to the density of the diamond lattice. In

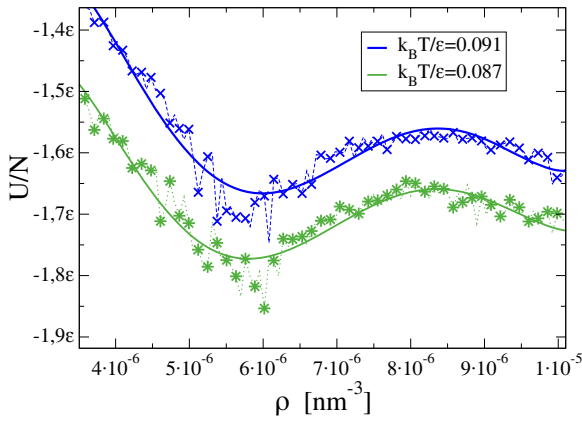


Fig. 4. Potential energy per particle as a function of ρ for two values of T . The lines are guide to the eyes.

models with softer interactions, an additional secondary minimum appears at even higher densities, which it has been associated with the network inter-penetrating structure. The presence of a region of negative curvature in the ρ dependence of the potential energy can be considered as a possible precursor of a thermodynamic instability [45].

Figure 4 shows that in the present model a clear maximum is observed in the ρ dependence of the potential energy, strongly supporting the possibility that in this model a liquid-liquid transition could be observed at low T . As expected, the first minimum is located at approximately the diamond density, *e.g.* the density at which a fully bonded network may form.

4.3 Phase behaviour

The probability $P(N)$ of observing N particle in a fixed volume V (in the μVT ensemble) provides information on the phase behaviour. In single-phase conditions, $P(N)$ has a single maximum centred on the average number of particles $\langle N \rangle$ from which the corresponding system density $\rho = \langle N \rangle / V$ can be estimated. On approaching a critical point, $P(N)$ develops a two peak structure which become more and more resolved on cooling. The value of the chemical potential for which the two peaks have equal area provides the coexistence μ , while the number of particles averaged over each peak provides the values of the two coexisting densities.

We find that $P(N)$ shows a bimodal shape under two different conditions: at low T and low ρ we observe the standard gas-liquid (*gl*) phase separation, with a (scaled) critical temperature $k_B T_{gl}^c / \epsilon \approx 0.096$ and a critical density of about $\rho_{gl}^c \approx 2.96 \cdot 10^{-6} \text{ nm}^{-3}$. We also find an additional phase separation, involving two distinct liquid (*ll*) phases at a critical temperature $k_B T_{ll}^c / \epsilon \approx 0.085$ and a critical density of about $\rho_{ll}^c \approx 8.53 \cdot 10^{-6} \text{ nm}^{-3}$. Indeed, in both cases (see fig. 5(a), (b)), at constant T and μ , $P(N)$ develops a two peak structure. The phase diagram thus contains two distinct instability regions, associated to the two transitions. For $T < T_{ll}^c$ on increasing density,

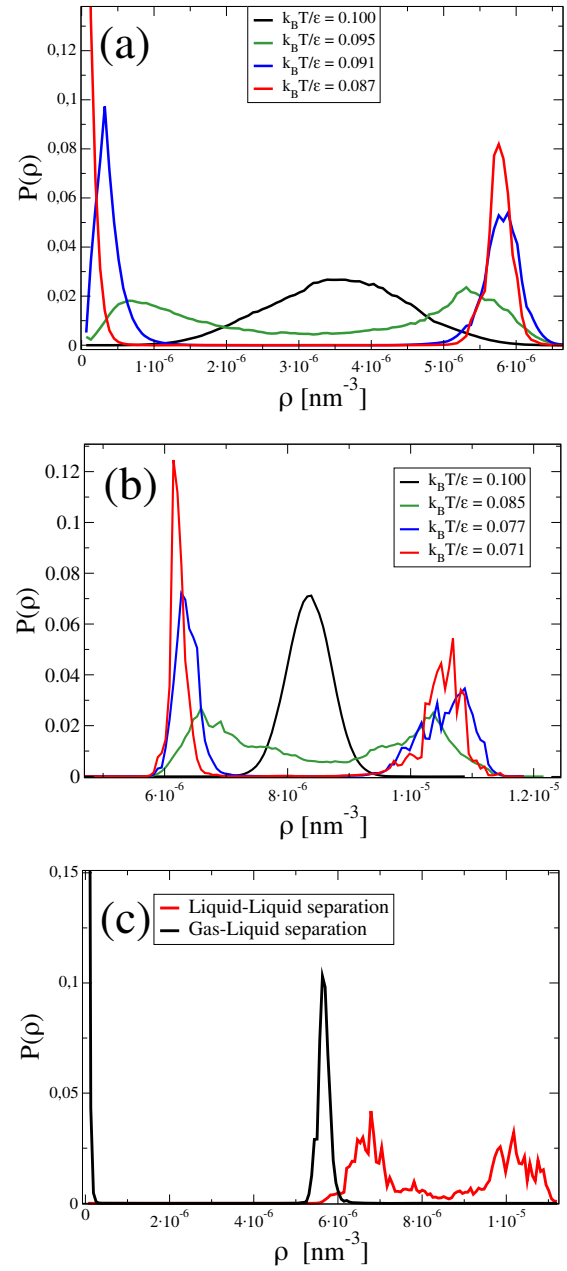


Fig. 5. Distribution of density fluctuations $P(\rho)$ evaluated via grand-canonical simulations at $V = 1.56 \cdot 10^7 \text{ nm}^3$. All distributions are centred around the critical density. (a) Distributions around the gas-liquid transition. (b) Distributions around the liquid-liquid transition. High T values show a single peak so no phase separation is observed. The onset of a two-peak structure in $P(\rho)$ on cooling indicates the onset of a phase separation. (c) Comparison between the gas-liquid $P(\rho)$ and the liquid-liquid $P(\rho)$ at $k_B T / \epsilon = 0.077$. The values of the chemical potentials are $\beta \mu_{gl} = -14.32$ and $\beta \mu_{ll} = -13.36$, respectively.

the system moves from the gas phase to the low-density liquid (LDL) phase which transforms again, on further increasing ρ , in the high-density liquid (HDL) (see fig. 5(c)). The resulting phase diagram is shown in fig. 6.

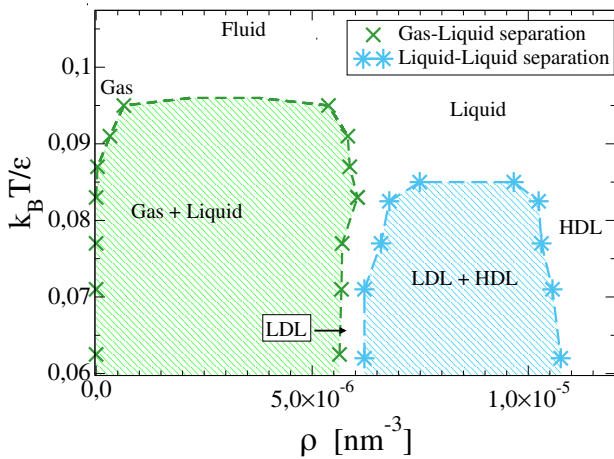


Fig. 6. Phase diagram of the model: the standard gas-liquid phase separation takes place at a (scaled) critical temperature $k_B T_{gl}^c / \epsilon \approx 0.096$ and a critical density of $\rho_{gl}^c \approx 2.96 \cdot 10^{-6} \text{ nm}^{-3}$. Then the system encounters an additional phase separation, involving two distinct liquid phases at a critical temperature $k_B T_{ll}^c / \epsilon \approx 0.085$ and a critical density of $\rho_{ll}^c \approx 8.53 \cdot 10^{-6} \text{ nm}^{-3}$. The green (gas-liquid) and blue (liquid-liquid) regions indicate thermodynamically unstable states.

5 Conclusions

In this article we have demonstrated that model particles with the same shape and attractive spots of the recently created DNA-decorated tetrahedra origami show *in silico* a liquid-liquid critical point. The model particle is composed of a tetrahedral scaffold formed by rigid cylinders with square-well interaction sites at the vertices. The excluded volume of the particles, significantly smaller than the one of spheres, allows for particle interpenetration (softness), the first criteria requested for the observation of a liquid-liquid critical point. The tetrahedral coordination and the intermediated bond flexibility which results from the square-well interaction satisfy the second criteria for the existence of a LL transition. In this respect, the observation of the LLCP, not only strengthens the generality of the LL phenomenon, providing a single-component model with a clear LL transition, but it has also the additional value of providing a first strong confirmation of the ideas presented in ref. [31].

The strong similarity between the investigated model and the DNA-decorated tetrahedra origami hopefully will be of guidance to transform this *in silico* demonstration into a real-world realisation, providing the first experimental observation of a liquid-liquid transition in a tetrahedral particles system.

F.S. acknowledges support from ETN-COLLDENSE (H2020-MCSA-ITN-2014, Grant No. 642774).

References

1. Sander Woutersen, Michiel Hilbers, Zuofeng Zhao, C. Austen Angell, arXiv preprint arXiv:1605.08985 (2016).
2. Paola Gallo, Francesco Sciortino, Phys. Rev. Lett. **109**, 177801 (2012).
3. T.A. Kesselring, G. Franzese, S.V. Buldyrev, H.J. Herrmann, H.E. Stanley, Sci. Rep. **2**, 474 (2012).
4. Ken-ichiro Murata, Hajime Tanaka, Nat. Mater. **11**, 436 (2012).
5. Yaping Li, Jicun Li, Feng Wang, Proc. Natl. Acad. Sci. U.S.A. **110**, 12209 (2013).
6. Jeremy C. Palmer, Fausto Martelli, Yang Liu, Roberto Car, Athanassios Z. Panagiotopoulos, Pablo G. Debenedetti, Nature **510**, 385 (2014).
7. Yang Liu, Jeremy C. Palmer, Athanassios Z. Panagiotopoulos, Pablo G. Debenedetti, J. Chem. Phys. **137**, 214505 (2012).
8. Jeremy C. Palmer, Roberto Car, Pablo G. Debenedetti, Farad. Discuss. **167**, 77 (2013).
9. Peter H. Poole, Richard K. Bowles, Ivan Saika-Voivod, Francesco Sciortino, J. Chem. Phys. **138**, 034505 (2013).
10. Peter H. Poole, Francesco Sciortino, Ulrich Essmann, H. Eugene Stanley, Nature **360**, 324 (1992).
11. Frank H. Stillinger, Aneesur Rahman, J. Chem. Phys. **60**, 1545 (1974).
12. E.A. Jagla, Phys. Rev. E **63**, 061509 (2001).
13. Giancarlo Franzese, Gianpietro Malescio, Anna Skibinsky, Sergey V. Buldyrev, H. Eugene Stanley *et al.*, Nature **409**, 692 (2001).
14. Dario Corradini, Sergey V. Buldyrev, Paola Gallo, H. Eugene Stanley, Phys. Rev. E **81**, 061504 (2010).
15. James N. Glosli, Francis H. Ree, Phys. Rev. Lett. **82**, 4659 (1999).
16. M. Van Thiel, F.H. Ree, Phys. Rev. B **48**, 3591 (1993).
17. Srikanth Sastry, C. Austen Angell, Nat. Mater. **2**, 739 (2003).
18. Vishwas V. Vasisht, Shibu Saw, Srikanth Sastry, Nat. Phys. **7**, 549 (2011).
19. Martin Beye, Florian Sorgenfrei, William F. Schlotter, Wilfried Wurth, Alexander Föhlisch, Proc. Natl. Acad. Sci. U.S.A. **107**, 16772 (2010).
20. Frank H. Stillinger, Thomas A. Weber, Phys. Rev. B **31**, 5262 (1985).
21. Katharina Vollmayr, Walter Kob, Kurt Binder, Phys. Rev. B **54**, 15808 (1996).
22. Ivan Saika-Voivod, Francesco Sciortino, Peter H. Poole, Phys. Rev. E **63**, 011202 (2000).
23. Osamu Mishima, H. Eugene Stanley, Nature **396**, 329 (1998).
24. Osamu Mishima, H. Eugene Stanley, Nature **392**, 164 (1998).
25. Osamu Mishima, Phys. Rev. Lett. **85**, 334 (2000).
26. Thomas Loerting, Christoph Salzmann, Ingrid Kohl, Erwin Mayer, Andreas Hallbrucker, Phys. Chem Chem. Phys. **3**, 5355 (2001).
27. Katrin Amann-Winkel, Catalin Gainaru, Philip H. Handle, Markus Seidl, Helge Nelson, Roland Böhmer, Thomas Loerting, Proc. Natl. Acad. Sci. U.S.A. **110**, 17720 (2013).
28. Kurt Binder, Walter Kob, *Glassy Materials and Disordered Solids: An Introduction to Their Statistical Mechanics* (World Scientific, 2011).

29. Chia Wei Hsu, Francis W. Starr, Phys. Rev. E **79**, 041502 (2009).
30. Chia Wei Hsu, Julio Largo, Francesco Sciortino, Francis W. Starr, Proc. Natl. Acad. Sci. U.S.A. **105**, 13711 (2008).
31. Frank Smallenburg, Laura Filion, Francesco Sciortino, Nat. Phys. **10**, 653 (2014).
32. Francis W. Starr, Nat. Phys. **10**, 628 (2014).
33. Flavio Romano, Eduardo Sanz, Francesco Sciortino, J. Chem. Phys. **132**, 184501 (2010).
34. Flavio Romano, Eduardo Sanz, Francesco Sciortino, J. Chem. Phys. **134**, 174502 (2011).
35. Frank Smallenburg, Francesco Sciortino, Nat. Phys. **9**, 554 (2013).
36. Francis W. Starr, Francesco Sciortino, Soft Matter **10**, 9413 (2014).
37. Frank Smallenburg, Francesco Sciortino, Phys. Rev. Lett. **115**, 015701 (2015).
38. Wenyan Liu, Miho Tagawa, Huolin L. Xin, Tong Wang, Hamed Emamy, Huilin Li, Kevin G. Yager, Francis W. Starr, Alexei V. Tkachenko, Oleg Gang, Science **351**, 582 (2016).
39. Ivan Saika-Voivod, Frank Smallenburg, Francesco Sciortino, J. Chem. Phys. **139**, 234901 (2013).
40. Peter Virnau, Marcus Müller, J. Chem. Phys. **120**, 10925 (2004).
41. Jean-Pierre Hansen, Ian R. McDonald, *Theory of Simple Liquids* (Elsevier, 1990).
42. Ivan Saika-Voivod, Francesco Sciortino, Peter H. Poole, Phys. Rev. E **69**, 041503 (2004).
43. Francesco Sciortino, Ivan Saika-Voivod, Peter H. Poole, Phys. Chem. Chem. Phys. **13**, 19759 (2011).
44. José L.F. Abascal, Carlos Vega, J. Chem. Phys. **133**, 234502 (2010).
45. Peter H. Poole, Francesco Sciortino, Ulrich Essmann, H. Eugene Stanley, Phys. Rev. E **48**, 3799 (1993).